Prediction of TiO2 Nanoparticle Phase and Shape Transitions Controlled by Surface Chemistry

ARTICLE *in* NANO LETTERS · AUGUST 2005

Impact Factor: 13.59 · DOI: 10.1021/nl050355m · Source: PubMed

2 AUTHORS, INCLUDING:

Amanda S Barnard

The Commonwealth Scientific and Industrial …

180 PUBLICATIONS **4,291** CITATIONS

NANO LETTERS

2005
Vol. 5, No. 7
1261−1266

Prediction of TiO_2 Nanoparticle Phase and Shape Transitions Controlled by Surface Chemistry

A. S. Barnard*,†,‡ and L. A. Curtiss‡,§

Center for Nanoscale Materials, Materials Science and Chemistry Divisions, Argonne National Laboratory, 9700 South Cass Ave, Argonne, Illinois 60439

Received February 24, 2005; Revised Manuscript Received May 4, 2005

ABSTRACT

The effects of surface chemistry on the morphology and phase stability of titanium dioxide nanoparticles have been investigated using a thermodynamic model based on surface free energies and surface tensions obtained from first principles calculations. It has been found that surfaces representing acidic and alkaline conditions have a significant influence on both the shape of the nanocrystals and the anatase-to-rutile transition size. The latter introduces the possibility of inducing phase transitions by changing the surface chemistry.

The current interest in titanium dioxide nanoparticles for advanced photochemical applications[1] has prompted a number of studies to analyze the properties of titanium dioxide surfaces under various conditions, such as acids and alkalines.[2,3] TiO_2 nanoparticles are typically grown via sol−gel synthesis, and while the finite size is instrumental in facilitating many new technologies, the phase and morphology have been found to be critical parameters in determining their suitability for particular applications.[4−8]

At ambient pressures and temperatures the rutile phase is the thermodynamically stable phase of TiO_2 (macroscopically);[9] however, anatase has been found to be a majority product of nanoscale natural and synthetic samples.[10−12] A number of authors[13−16] have shown that the synthesis of nanocrystalline TiO_2 consistently resulted in anatase nanoparticles, which transformed to rutile upon reaching a particular size. Experimentally, the size range of the anatase-to-rutile phase transition for hydrothermal samples (at ∼650−800 K) has been predicted to be approximately 11.4−17.6 nm,[13] although the precise size has been found to depend on parameters such as temperature,[17,18] impurities,[19−21] reaction atmosphere,[22,23] and synthesis conditions.[24−28]

It has been known for some time that the pH value of the sol−gel is a decisive factor for controlling the final particle size,[29] shape,[30] phase[29,31,32] and agglomeration.[33] In the case of anatase (for example), alkaline conditions have been reported to result in small cubic-like nanocrystals with {112} and {103} facets,[34] hexagonal nanocrystals,[35] or short rod-like nanocrystals with {010}, {101}, and {001} facets.[2,35] In contrast, acidic conditions reportedly result almost exclusively in truncated tetragonal bipyramidal nanocrystals with {101}, {001}, and {010} facets.[28,34,36] It has also been shown that the formation rate of anatase is dependent on pH,[37] and an excess dilution of the particle density during synthesis causing partial dissolution of TiO_2 nanocrystals[34] (or melting[33]), may result in spherical nanoparticles. In each case, however, the final nanomorphology is dependent upon the value of the pH, and hence the properties will be sensitive to the resultant chemistry at the surfaces.[6,37,38]

In present study, a thermodynamic model[39] based on the free energy of (arbitrary) nanocrystals as a function of size and shape has been systematically used to determine the minimum energy morphology of anatase and rutile nanocrystals with varying surface chemistry. The surface free energies and the surface tensions for the (100), (001), and (101) surfaces of anatase and the (100), (110), and (011) surfaces of rutile have been presented elsewhere,[40] calculated using first principles methods, and terminated with adsorbates representative of acidic and alkaline conditions.

In this paper we used these values to investigate the effect of surface chemistry on the anatase-to-rutile phase transition and found a most startling result. Not only did the phase transition exhibit a definite dependence on the ratio of O to H atoms in surface adsorbates but also (as a consequence of this dependence) the possibility exists for reversible, surface chemistry induced phase transitions in pre-grown nanoparticles.

As mentioned above, we have used a shape dependent thermodynamic model[39] based on the Gibbs free energy G_x° of a nanoparticle of material x ($x = \mathscr{A}$ for anatase, and $x = \mathscr{R}$ for rutile), described by a sum of contributions from the

* Corresponding author. E-mail: amanda.barnard@anl.gov.
† Center for Nanoscale Materials.
‡ Materials Science Division.
§ Chemistry Division.

10.1021/nl050355m CCC: $30.25
Published on Web 06/03/2005

particle bulk and surfaces such that

$$G_x^\circ = G_x^{\text{bulk}} + G_x^{\text{surface}} \tag{1}$$

This is then further defined in terms of the surface energy γ_{xi} for each crystallographic surface i, weighted by the factors f_i, such that $\sum_i f_i = 1$. Hence,

$$G_x^\circ = \Delta_f G_x^\circ + \frac{M}{\rho_x}(1 - e)[q\sum_i f_i \gamma_{xi}] \tag{2}$$

where $\Delta_f G_x^\circ$ is the standard free energy of formation of the bulk (macroscopic) material,[41] M is the molar mass, ρ_x is the density, and e is the volume dilation induced by the surface tension. In general, the surface-to-volume ratio q and the weighting factors f_i must be calculated explicitly for each shape and the facet therein. In this model the size dependence is introduced not only by the surface-to-volume ratio q but also by the reduction of e as the crystal grows larger. The shape dependence is also introduced by q, as well as the weighted sums of the surface energies and the surface tensions.[39]

It has previously been shown[39] that the Laplace−Young equation is suitable for approximating the volume dilation of faceted nanocrystals, and that the edge and corner effects are limited over a diameter of approximately 2 nm.[39,42] Therefore, the volume dilation due to the surface tension, with the compressibility $\beta = 1/B_0$ (previously calculated[42] by fitting to the Vinet equation of state[43]), is defined as

$$e = \frac{2\beta\sigma_x}{R} \tag{3}$$

Here, σ_x is obtained by summing over the (weighted) surface tensions of the crystallographic surfaces present on the nanocrystal,

$$\sigma_x = \sum_i f_i \sigma_{xi} \tag{4}$$

where σ_{xi} is the surface tension of the particular crystallographic surface i of phase x.

As mentioned above, the surface energies and surface tensions have been calculated elsewhere,[40] using density functional theory (DFT) within the generalized gradient approximation (GGA), with adsorbates representing acidic, neutral, and alkaline conditions.[40] From experiment, it is known that the structure of surfaces are determined by acid−base equilibria involving TiOH surface hydroxyl groups.[44−49] Under neutral pH conditions, the surfaces are found to be terminated with water adsorbates (either as molecular H_2O or as dissociated $OH^- + H^+$) capping the under-coordinated surface sites.[44,45] When in acidic solutions protonation occurs, with the (lowest pH) limiting case occurring when all under-coordinated surface sites are protonated. Similarly, when in alkaline solution, the surfaces are deprotonated,[47,50] and the (upper pH) limiting case involves total deprotonation and all under-coordinated surface sites terminated with O^-.

Therefore, the surface acidity is primarily described by the ratio of H and O on the surface. In reference 40 such variations in surface chemistry were introduced by varying the ratio of hydrogen to oxygen in a complete monolayer of adsorbates, thereby representing different degrees of surface acidity. Fully hydrogenated (H-terminated) surfaces were used to represent highly acidic surfaces; hydrogen-rich (with respect to H_2O terminations) surfaces were used to represent moderately acidic surfaces; hydrated (H_2O-terminated) surfaces were used to represent neutral surfaces; hydrogen-poor (with respect to H_2O terminations) surfaces were used to represent moderately alkaline surfaces; and oxygenated (O-terminated) surfaces were used to represent highly alkaline surfaces. The corresponding chemical potentials were then constructed with respect to the neutral (hydrated) surfaces, and the surface energies and surface tensions were calculated using DFT GGA. More details are contained within ref 40; however, for convenience, the values of each set of surface energies and surface tensions, with each type or surface chemistry, are listed in Table 1.

Taking the values for the surface energies, the standard method for determining the equilibrium morphology of a material is to generate the Wulff construction.[51] However, as the Wulff construction does not take into account the effects of surface tension, the morphology of nanocrystals may deviate from this shape. Using the model outlined above, it is possible to optimize the shape of nanoparticles as a function of size,[52] or other parameters such as temperature. Here, we have performed such an optimization as a function of size, since the γ_{xi} and σ_{xi} in ref 40 were calculated at $T = 0$, and it has been shown by Zhang and Banfield[14] that the change in the surface energies of TiO_2 nanoparticles with temperature is of the order of 10^{-4} J/m^2. It has therefore been assumed here that variations in nanomorphology due to temperature effects will be negligible.

In nature, rutile crystals may vary in shape between long acicular (needle-like) crystals to a short blocky habit, due to the morphology being dominated by an (open) tetragonal prismatic form. Unfortunately, because the form is open, optimization of aspect-ratio (or length) for the rutile crystals using the model outlined above is not possible.[52] Therefore, the traditional Wulff construction has been used to define the shape and aspect-ratio of the rutile nanoparticles during the remainder of this study.

In nature, anatase crystals may exhibit a (closed) tetragonal bipyramidal form, as shown in wire-frame in Figure 1, or a truncated bipyramid (or bifrustum), with square facets in the (001) and (00$\bar{1}$) planes, as displayed as the interior solid in Figure 1. In this case, the morphology of anatase nanocrystals may be defined in terms of two independent length parameters **A** and **B**. The side of this bipyramidal is denoted **A**. The side of this "truncation" facet is denoted **B**. The degree of truncation may therefore be described by the size of **B** with respect to **A** (where $0 \le \mathbf{B} \le \mathbf{A}$).[52,53]

Table 1. Surface Energy γ_{xi} (and surface tension σ_{xi}) for Selected Anatase and Rutile Surfaces (in J/m^2), Calculated in Reference 40, for Each Type of Surface Chemistry[a]

	hydrogenated	hydrogen-rich	hydrated	hydrogen-poor	oxygenated
anatase					
(001)	1.88 (0.91)	2.28 (0.41)	1.55 (−0.37)	1.89 (0.83)	2.55 (1.28)
(100)	1.41 (−0.19)	1.67 (−0.08)	1.113 (−0.59)	1.58 (0.04)	1.53 (0.35)
(101)	1.14 (0.09)	1.41 (0.21)	1.03 (0.45)	1.50 (0.54)	2.07 (0.28)
rutile					
(100)	3.07 (0.80)	− (−)	1.57 (0.61)	1.91 (0.49)	2.55 (0.63)
(110)	1.72 (1.27)	1.60 (1.65)	1.08 (0.92)	1.30 (1.69)	1.60 (0.67)
(011)	2.55 (1.38)	2.94 (−2.63)	1.79 (1.36)	3.58 (−1.33)	4.02 (−0.55)

[a] The σ_{xi} values are given in brackets. Note that results for the rutile (100) surface in hydrogen-rich conditions are unavailable, since this surface was found to be unstable with respect to H_2O desorption.

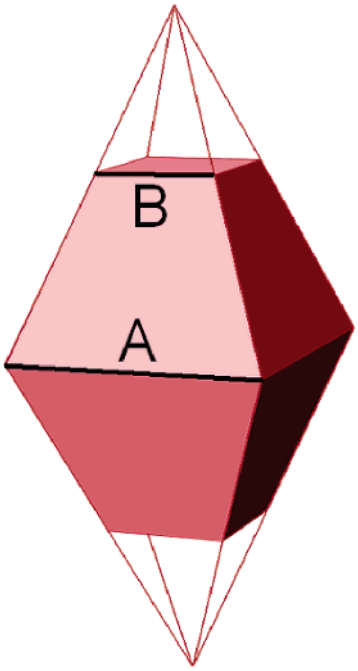

Figure 1. An anatase tetragonal {101} bipyramid is shown in outline, and an example of the bifrustum formed by addition of (001) and (00$\bar{1}$) truncation facets is shown as the interior solid. The side lengths labeled **A** and **B** are used to define the degree of truncation.

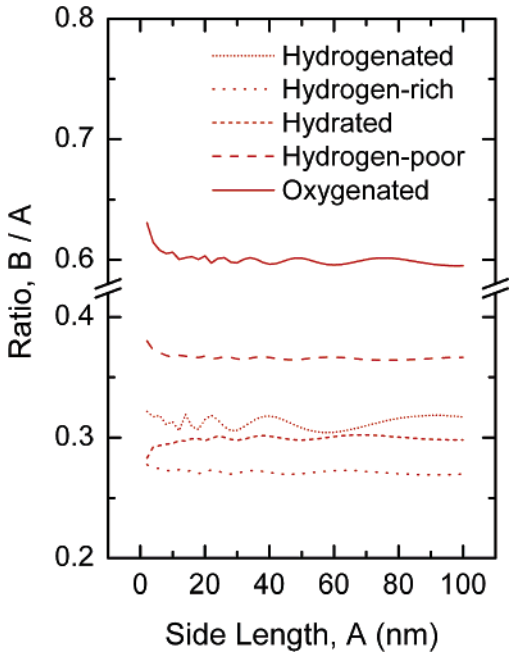

Figure 2. Plot of the optimized ratio **B**/**A** for anatase nanocrystals with each of the various surface chemistries defined in ref 40, with a side length **A** = 2 to 100 nm. The facet edges **A** and **B** are defined in Figure 1.

By defining all the geometric parameters, such as the volume and surface area of the various facets in terms of the ratio **B**/**A**, the total Gibbs free energy for anatase $G^\circ_{\mathcal{A}}$ was minimized with respect to this new variable. This is equivalent to optimizing the shape with respect to the nanocrystal aspect ratio. To achieve this, a numerical minimization was performed using a conjugate gradient scheme, to identify the value of **B**/**A** that produces a shape that is lower in energy than the Wulff construction as a function of size. Figure 2 shows a plot of the optimized **B**/**A** for sizes **A** = 2 to 100 nm.

From Figure 2, it may be seen that the degree of truncation fluctuates considerably as a function of a size for the fully hydrogenated (and to a lesser extent the oxygenated particles), but fluctuates very little for particles with a mix of O and H in the adsorbates. In addition to this, the degree of truncation varies depending upon the surface chemistry, although not in a predicable way. The oxygenated and hydrogen-poor surfaces show the greatest degree of truncation (approximately **B**/**A** = 0.59 and 0.37, respectively); however, the degree of truncation does not simply decrease with increasing fraction of hydrogen in the adsorbates. The results from Figure 2 were used to define the aspect-ratio of the anatase nanoparticles during the remainder of this study.

Using the results from ref 40 given in Table 1 for anatase and rutile, the final shapes predicted for each type of surface chemistry as defined above (with a side length **A** ≤ 15 nm) are shown in Figure 3. The effect of changing the surface chemistry upon the shape of the anatase and rutile nanoparticles is readily apparent. When hydrogen is dominant on the surface (or there is a greater fraction of hydrogen present in the adsorbates), there is little change in the shape of the nanocrystals with respect to the (neutral) water terminated nanoparticles; however, when oxygen is dominant on the surface, the nanoparticles of both polymorphs become elongated. This is consistent with experimental findings.[2,28,34−36]

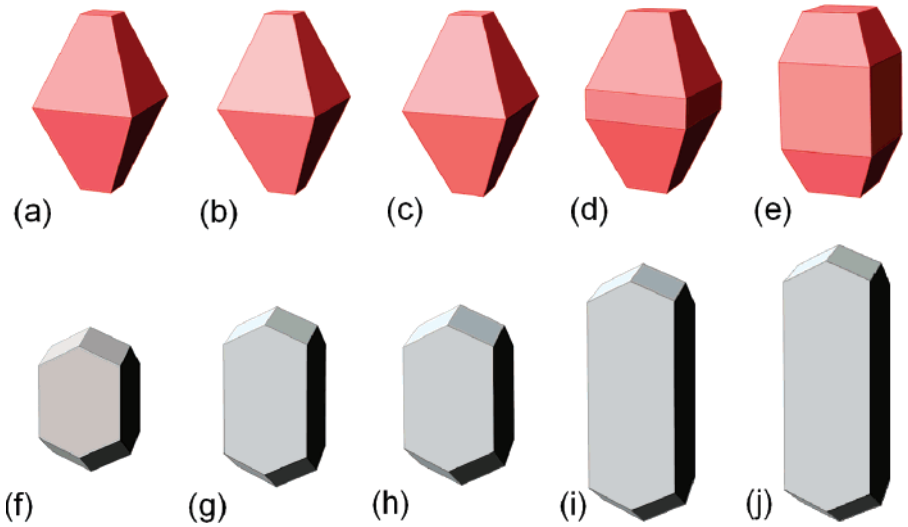

Figure 3. Morphology predicted for anatase (top) with (a) hydrogenated surfaces (b) with hydrogen-rich surface adsorbates, (c) hydrated surfaces, (d) hydrogen-poor adsorbates, and (e) oxygenated surfaces, and rutile (bottom) with (f) hydrogenated surfaces, (g) with hydrogen-rich surface adsorbates, (h) hydrated surfaces, (i) hydrogen-poor adsorbates, and (j) oxygenated surfaces.

It is also important to note that the anatase nanocrystals with hydrogen-poor surfaces, and especially with oxygenated surfaces, have developed facets in the ⟨100⟩ and ⟨010⟩ directions. These appear as the "belt" around the center of the nanoparticles, and were present to some extent in the Wulff construction (for macroscopic anatase crystals). Therefore, the procedure described above was repeated to optimize the size of these facets by using an analogous truncation length **C** and optimizing the parameter **C**/**A**. The morphologies shown in Figures 3d and 3e are a result of both **B**/**A** and **C**/**A** optimizations.

For each of the nanocrystals shown in Figure 3, the value of $G^{\circ}_{\mathscr{A}}$ and $G^{\circ}_{\mathscr{R}}$ (from eq 2) were calculated and plotted together as a function of the number of TiO_2 units, by using the appropriate γ_{xi} and σ_{xi} from Table 1.[40] These plots are shown in Figure 4 for each type of surface chemistry. The intersection points in each plot denote the phase transition sizes, which have been conveniently converted to the equivalent average anatase nanoparticle diameter.

As shown in Figure 4(a−e), the phase transitions for TiO_2 nanoparticles with hydrogenated, hydrogen-rich, hydrated, hydrogen-poor, and oxygenated surfaces occur at sizes of approximately 22.7, 18.4, 15.1, 13.2, and 6.9 nm, respectively. This is not to say that anatase nanoparticles may not exist above these sizes, but above these sizes they will be metastable with respect to transformation to rutile. These results clearly demonstrate a dependence of the phase transition size on composition of the adsorbates. The anatase nanoparticles are stabilized by surface adsorbates containing a large fraction of hydrogen, whereas rutile nanoparticles are stabilized by surface adsorbates containing a large fraction of oxygen. More specifically, by plotting the phase transition size versus the fraction of hydrogen in the adsorbates, a very good empirical fit was obtained using the expression

$$S = S_0 \exp\{5s/4\} \tag{5}$$

where S is the phase transition size in nanometers, s is the fraction of hydrogen in the adsorbates, and S_0 is the phase transition size when $s = 0$.

A more direct comparison of the graphs contained in Figure 4 reveals another interesting result. A consequence of the dependence of the anatase-to-rutile phase transition on the surface chemistry, is the possibility is introduced for phase transitions to be induced by a change in the absorbed groups on the surfaces. Referring to Figure 5, which shows the free energy for anatase (red) and rutile (black) with hydrogen-rich, hydrated (neutral), hydrogen-poor surface chemistry, consider the vertical guide-line at 45 000 TiO_2 units. Beginning with hydrogen-rich surfaces (solid lines in Figure 5), anatase is thermodynamically stable. As the surface chemistry is neutralized (moving the eye upward, along the guide-line) to correspond with hydrated surfaces (deprotonation) as shown by the dashed lines in Figure 5, the anatase phase remains stable. However, further deprotonation induces a phase transition to rutile, since with hydrogen-poor surface chemistry (the dotted lines in Figure 5), rutile is thermodynamically preferred at a size of 45 000 TiO_2 units.

Then, consider the same procedure following the guideline at 75 000 TiO_2 units. Beginning with hydrogen-rich surfaces, anatase is again thermodynamically stable. As the surface undergoes deprotonation, the anatase phase transforms to rutile, since for hydrated surfaces, rutile is thermodynamically preferred at a size of 75 000 TiO_2 units. This phase transition for nanoparticles containing 75 000 TiO_2 units occurs at an earlier stage of deprotonation than nanoparticles containing 45 000 TiO_2 units. These results indicate not only that the opportunity exists for surface chemistry induced phase transitions to occur, but that these types of phase transitions are themselves, size dependent.

Surface chemistry induced transformations in TiO_2 nanostructures have been observed experimentally. In a recent study by Saponjic et al.,[49] scrolled TiO_2 nanotubes with the anatase structure were synthesized in alkaline solution

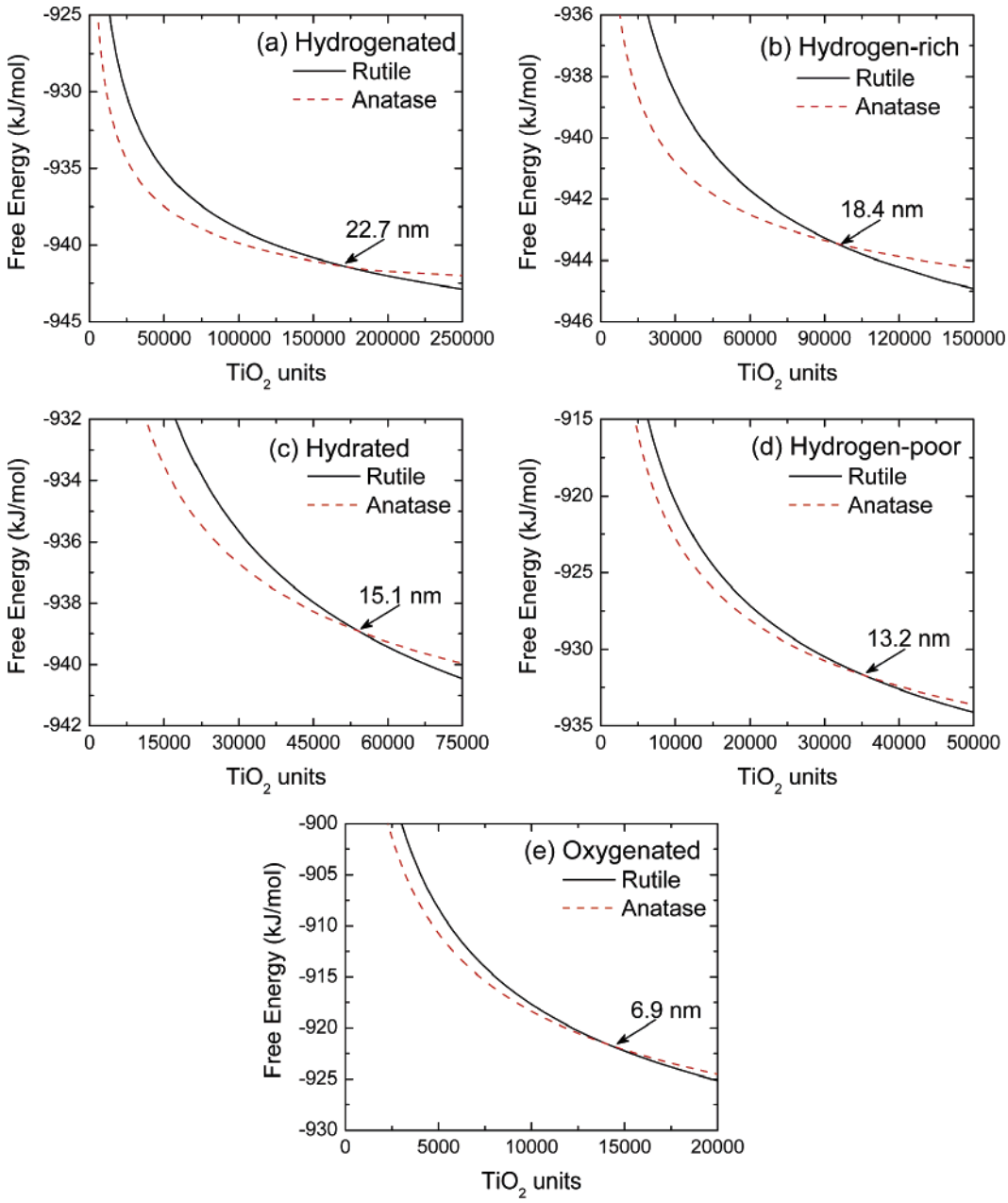

Figure 4. Free energy as a function of the number of TiO_2 units for anatase and rutile (a) with hydrogenated surfaces (b) with hydrogen-rich surface adsorbates, (c) hydrated surfaces, (d) hydrogen-poor adsorbates, and (e) oxygenated surfaces, calculated using the shapes given in Figure 3 and the values of γ_{xi} and σ_{xi} from ref 40. The intersection points indicate the phase transitions.

(pH = 11) and prompted to unscroll by charging the under-coordinated surface sites with protons (to a pH of 2). This unscrolling was accompanied by a phase transition, resulting in nanosheets with the rutile structure. Both the scrolling and unscrolling processes and the accompanying phase transitions were found to be reversible, since increasing the pH from 2 to 11 removed the adsorbed protons, provided a driving force for self-coiling of the TiO_2 nanosheets and the reestablishment of the anatase structure.[49] These results were explained by a plot of the energetics as a function of the surface area-to-volume ratios, and transitions were identified between metastable states. Further details of this experimental work, and the accompanying theoretical explanations may be found within ref 49, which provides evidence of a surface chemistry induced phase transition in nanostructured TiO_2.

A number of important conclusions may be drawn from the present study. By using a thermodynamic model (capable of describing the free energy of nanoparticles as a function of size, shape and surface chemistry), and surface energies and surface tension calculated for anatase and rutile surfaces terminated by adsorbates with varying fractions of hydrogen and oxygen,[40] we have shown that both the shape and phase stability of TiO_2 nanoparticles are highly dependent on surface chemistry. In the case of hydrogenated, hydrogen-rich, and hydrated surfaces, our model predicts that the shape of anatase and rutile nanoparticles vary very little with surface chemistry (with only slight changes in the in aspect ratio evident); however, in the case of hydrogen-poor and oxygenated surfaces, nanocrystals of both polymorphs become elongated.

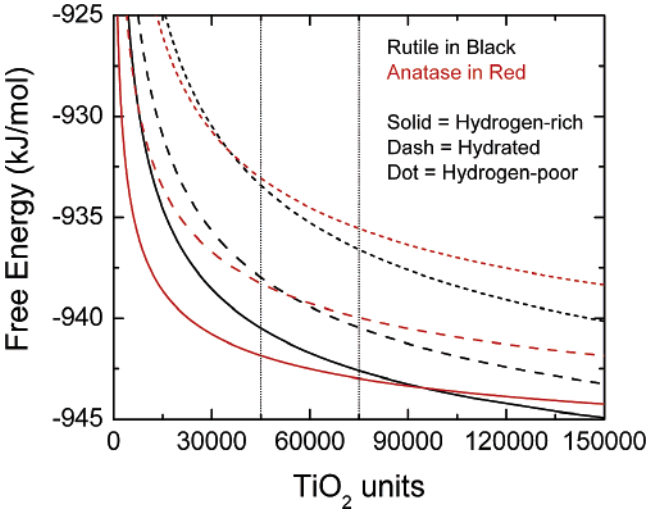

Figure 5. Free energy as a function of the number of TiO_2 units for anatase and rutile with hydrogen-rich, hydrated, and hydrogen-poor surfaces. Vertical guidelines assist in the comparison of different stable phases at 45 000 and 75 000 TiO_2 units during deprotonation (moving from the bottom upward).

It was also found that anatase nanoparticles are stabilized by surface adsorbates containing a large fraction of hydrogen, whereas rutile nanoparticles are stabilized by surface adsorbates containing a large fraction of oxygen. It is therefore not surprising that anatase nanoparticles are typically grown in acidic solution.[2,29,30,37] Empirically, an exponential expression was found to relate the phase transition size with the fraction of hydrogen present on the surfaces. As a consequence of this dependence of the anatase-to-rutile phase transition on the surface chemistry, our model predicts that phase transitions may be induced by changing the adsorbed groups on the surfaces. This suggests new avenues for the control and manipulation of the shape and phase of TiO_2 at the nanoscale.

Acknowledgment. This work has been supported by the U.S. Department of Energy, Office of Basic Energy Sciences, under contract W-31-109-ENG-38. Computational resources for this project have been supplied by Argonne National Laboratory − Laboratory Computing Resource Center, Pacific Northwest National Laboratory Molecular Science Computing Facility and the U.S. Department of Energy National Energy Research Scientific Computing Center. We would also like to acknowledge Tijana Rajh and Zoran Saponjic from ANL for advice regarding links with experiment, and Peter Zapol.

References

(1) Zhang, W. F.; Zhang, M. S.; Yin Z.; Chen, Q. *Appl. Phys. B* **2000**, *70*, 261.
(2) Sugimoto, T.; Okada, K.; Itoh, H. *J. Colloid Interface Sci.* **2003**, *193*, 140.
(3) Pottier, A.; Cassaignon, S.; Chanéac, C.; Villain, F.; Tronc, E.; Jolivet, J.-P. *J. Mater. Chem.* **2003**, *13*, 877.
(4) Chen, L. C.; Rajh, T.; Jäger, W.; Nedeljkovic, J. M.; Thurnauer, M. C. *J. Synchrotron. Radiat.* **1999**, *6*, 455.
(5) Rajh, T.; Nedeljkovic, J. M.; Chen, L. C.; Poluektov, O.; Thurnauer, M. C. *J. Phys. Chem. B* **1999**, *103*, 3515.
(6) Zhang, H.; Penn, R. L.; Hamers, R. J.; Banfield, J. F. *J. Phys. Chem. B* **1999**, *103*, 4656.
(7) Jang, K. D.; Kim, S.-K.; Kim, S.-J. *J. Nanoparticle Res.* **2001**, *3*, 141.
(8) Bullen H.; Garrett, S. *Nano Lett.* **2002**, *2*, 739.
(9) Muscat, J.; Swamy, V.; Harrison, N. M. *Phys. Rev. B* **2002**, *65*, 224112.
(10) Navrotsky, A.; Kleppa, O. J. *J. Am. Ceram. Soc.* **1967**, *50*, 626.
(11) Mitsuhashi, T.; Kleppa, O. J. *J. Am. Ceram. Soc.* **1979**, *62*, 356.
(12) Zhang, H.; Banfield, J. F. *J. Phys. Chem. B* **2000**, *104*, 3491.
(13) Gribb, A. A.; Banfield J. F. *Am. Mineral.* **1997**, *82*, 717.
(14) Zhang, H.; Banfield, J. F. *J. Mater. Chem.* **1998**, *8*, 2073.
(15) Navrotsky, A. *Thermochemistry of Nanomaterials in Nanoparticles the Environment*, *Reviews in Mineralogy Geochemistry*, Banfield, J. F., Navrotsky, A., Eds. *Mineralog. Soc. Am.*, 2001, Vol. 44.
(16) Zhang, H.; Finnegan, M.; Banfield, J. F. *Nano Lett.* **2001**, *1*, 81.
(17) Gourma, P. I.; Mills, M. J. *J. Am. Ceram. Soc.* **2001**, *84*, 619.
(18) Li, Y.; White, T.; Lim, S. H. *Rev. Adv. Mater. Sci.* **2003**, *5*, 211.
(19) Arroyo, R.; Córdoba, G.; Padilla, J.; Lara, V. H. *Mater. Lett.* **2002**, *54*, 397.
(20) Arbiol, J.; Cerdà, J.; Dezanneau, G.; Cirera, A.; Peiró, F.; Cornet, A.; Morante, J. R. *J. Appl. Phys.* **2002**, *92*, 853.
(21) Francisco, M. S. P.; Mastelaro, V. R. *Chem. Mater.* **2002**, *14*, 2514.
(22) Kittaka, S.; Matsuno K.; Takahara, S. *J. Solid State Chem.* **1997**, *132*, 447.
(23) Ahonen, P. P.; Kauppinen, E. I.; Joubert, J. C.; Deschanvres, J. L.; Van Tendeloo, G. *J. Mater. Res.* **2000**, *14*, 3938.
(24) Zhang, H.; Banfield, J. F. *J. Mater. Res.* **2000**, *15*, 437.
(25) Yoshinaka, M.; Hirota, K.; Yamaguchi, O. *J. Am. Ceram. Soc.* **1997**, *80*, 2749.
(26) Okada, K.; Yamamoto, N.; Kameshima, Y.; Yasumori, A. *J. Am. Ceram. Soc.* **2001**, *84*, 1591.
(27) Yang, J.; Mei, S.; Ferreira, J. M. F. *J. Am. Ceram. Soc.* **2000**, *83*, 1361.
(28) Zaban, A.; Aruna, S. T.; Tirosh, S.; Gregg, B. A.; Mastai, Y. *J. Phys. Chem. B* **2000**, *104*, 4130.
(29) Sugimoto, T.; Zhou, X.; Muramatsu, A. *J. Colloid Interface Sci.* **2003**, *259*, 43.
(30) Sugimoto, T.; Zhou, X.; Muramatsu, A. *J. Colloid Interface Sci.* **2003**, *259*, 53.
(31) Yin, H.; Wada, Y.; Kitamura, T.; Sumida, T.; Hasegawa, Y.; Yanagida, S. *J. Mater. Chem.* **2002**, *123*, 78.
(32) Li, Y.; White, T.; Lim, S. H. *J. Solid State Chem.* **2004**, *77*, 1372.
(33) Sugiyama, M.; Okazaki, H.; Koda, S. *Jpn. J. Appl. Phys.* **2002**, *41*, 4666.
(34) Gao, Y.; Elder, S. A. *Mater. Lett.* **2000**, *44*, 228.
(35) Chemseddine, A.; Mortiz, T. *Eur. J. Inorg. Chem.* **1999**, 235.
(36) Penn, R. L.; Banfield, J. F. *Geochim. Cosmochim. Acta* **1999**, *63*, 1549.
(37) Sugimoto, T.; Zhou, X.; Muramatsu, A. *J. Colloid Interface Sci.* **2002**, *252*, 339.
(38) Sugimoto, T.; Zhou, X. *J. Colloid Interface Sci.* **2002**, *252*, 347.
(39) Barnard, A. S.; Zapol, P. *J. Chem. Phys.* **2004**, *121*, 4276.
(40) Barnard, A. S.; Zapol, P.; Curtiss, L. A. *Surf. Sci.* **2005**, *58*, 2173.
(41) The experimental free energies of formation of anatase (rutile) $\Delta G^\circ_{f,\mathscr{A}}$ ($\Delta G^\circ_{f,\mathscr{R}}$) taken from the JANAF tables have been applied here, such that $\Delta G^\circ_{f,\mathscr{A}} = -9.491471 \times 10^{-2}$ mJ/mol ($\Delta G^\circ_{f,\mathscr{R}} = -9.539962 \times 10^{-2}$ mJ/mol). Chase, M. W.; Davies, C. A.; Downey, J. R.; Frurip, D. J.; McDonald, R. A.; Syverud, A. N. *J. Phys. Chem. Ref. Data* **1985**, *14* (Suppl. 1), 1680.
(42) Barnard, A. S.; Zapol, P. *Phys. Rev. B* **2004**, *702*, 35403.
(43) Vinet, P.; Rose, J. H.; Ferrante, J.; Smith, J. R. *J. Phys: Condes. Matter* **1989**, *1*, 1941.
(44) Diebold, U. *Surf. Sci. Rep.* **2003**, *48*, 53.
(45) Hoffmann, M. R.; Martin, S. T.; Choi, W.; Bahnemann, D. W. *Chem. Rev.* **1995**, *95*, 69.
(46) Thurnauer, M. C.; Rajh, T.; Tiede, D. M. *Acta Chem. Scan.* **1997**, *51* 610.
(47) Nakaoka, Y.; Nosaka, Y. *J. Photochem. Photobiol. A* **1997**, *110*, 299.
(48) Szczepankiewicz, S. H.; Moss, J. A.; Hoffmann, M. R. *J. Phys. Chem. B* **2002**, *106*, 7654.
(49) Saponjic, Z. V.; Dimitrijevic, N.; Tiede, D.; Goshe, A.; Zuo, X.; Chen, L.; Barnard, A. S.; Zapol, P.; Curtiss, L. A.; Rajh, T. *Adv. Mater.* **2005**, *17*, 965.
(50) Kasuga, T.; Hiramatsu, M.; Hoson, A.; Sekino, T.; Niihara, K. *Adv. Mater.* **1999**, *11*, 1307.
(51) Wulff, G. *Z. Kristallogr. Mineral* **1901**, *34*, 449.
(52) Barnard, A. S.; Zapol, P. *J. Phys. Chem. B* **2003**, *108*, 18345.
(53) Barnard, A. S.; Zapol, P.; Curtiss, L. A. *J. Chem. Theo. Comput.* **2005**, *1*, 107.

NL050355M